A Wideband Millimeter-wave Corrugated Horn at 30-50 GHz Taking Advantage of All-Metal 3D-Printing Fabrication

Haoran Kang, Keiko Kaneko, Ryo Sakai and Alvaro Gonzalez

***Abstract*—Development of commercial all-metal 3D printing technology provides a new fabrication method for wideband millimeter-wave corrugated horns up to 50 GHz. All-metal 3D printing has advantages of low cost, fast delivery, possibility of mass production, flexibility in fabrication of complicated geometries and good mechanical robustness compared with traditional fabrication techniques, such as direct machining or electroforming, or recently developed methods such as those relying on the assembly of platelets. In this letter, we report the development of a wideband millimeter-wave corrugated horn at 30-50 GHz (50% fractional bandwidth) based on commercial all-metal 3D printing technology. Measurement results of return loss and beam patterns show good performance and are also reported in this letter.**

***Index Terms*—3D printing, Horn antennas, Wideband antennas**

I. Introduction

CORRUGATED horns have been widely used as feeds for reflector antennas from microwave to submillimeter wavelengths. The basic theory of corrugated horns was established in the 70's [1]–[3]. After a decade of development, the early design methods of corrugated horns are well summarized in [4]. Because corrugated horns have good beam symmetry, low sidelobes and low Cross-polarization (XsP) level, they have important applications in the field of radio astronomy, satellite communication and earth observation.

For astronomical applications, wideband receivers are an important development direction, because they have the capability to capture celestial signals from a wider range of electromagnetic (EM) spectrum and increase the overall efficiency of these instruments. For this reason, wideband receivers have been proposed in the next generation millimeter-wave (mm-wave) interferometer projects, like the Atacama Large Millimeter/submillimeter Array (ALMA) 2030 [5] and the next generation Very Large Array (ngVLA) [6]. On the other hand, for large single-dish mm-wave telescopes, several Q-Band wideband receivers have also been developed [7], [8].

Commonly, mm-wave corrugated horns are fabricated by direct machining [9] or electroforming [10], but these fabrication techniques require medium to high cost and long delivery time. Recently developments propose the use of platelet technique to fabricate wideband mm-wave corrugated horns which is able to reduce the cost [11], [12], but the mechanical robustness during thermal cycling is one of the main concerns of this technique. Due to the active development of all-metal 3D printing technology, especially Powder Bed Fusion (PBF) [13], a metal 3D printed mm-wave corrugated horn at 35-50 GHz is reported in [14]. The measurement results in [14] show that the corrugated horns fabricated by commercial PBF machine can operate up to 50 GHz, and the corrugated horns have very similar performance to direct machining corrugated horns. Because the metal 3D printed horns are one-piece components, they have good mechanical robustness during thermal cycling. The cost also can be further reduced compared with platelet technique because 3D printing procedure is highly automatic which requires fewer human resources.

In this letter, we report the development of a wideband mm-wave corrugated horn at 30-50 GHz based on commercial PBF technology. This corrugated horn has a fractional bandwidth of 50% which is larger than the state-of-the-art corrugated horn based on PBF technology which has a fractional bandwidth of 35% [14]. Metal 3D printed corrugated horn has advantages of low cost, fast delivery, possibility of mass production, flexibility in fabrication of complicated geometries and good mechanical robustness. These advantages can promote the application of wideband mm-wave corrugated horn in large array astronomical receivers. A similar corrugated horn design can be further applied in Q-band satellite communication [15] and remote sensing for meteorology [16]. In these fields, the combination of reflector antennas and feed horns is the dominant design solution.

II. Wideband Corrugated Horn Design

In general, corrugated horns consist of two sections, namely throat section and flare section. The functions of throat section are broadband impedance matching and circular waveguide mode to the hybrid HE_{11} mode conversion, and the hybrid HE_{11} mode has a high coupling efficiency with fundamental Gaussian mode which is preferred in high performance astronomical receivers. The flare section guides the hybrid

This work was supported in part by JST SPRING, under Grant JPMJSP2108. *(Corresponding author: Haoran Kang)*

Haoran Kang is with the Institute of Astronomy, Graduate School of Science, The University of Tokyo, Mitaka 181-0015, Japan, and also with the National Astronomical Observatory of Japan, Mitaka 181-8588, Japan (e-mail: kang-haoran@g.ecc.u-tokyo.ac.jp).

Keiko Kaneko and Ryo Sakai are with the National Astronomical Observatory of Japan, Mitaka 181-8588, Japan (e-mail: keiko.kaneko@nao.ac.jp; ryo.sakai@nao.ac.jp).

Alvaro Gonzalez is with the National Astronomical Observatory of Japan, Mitaka 181-8588, Japan, and also with the Graduate University for Advanced Studies (SOKENDAI), Mitaka 181-8588, Japan (e-mail: alvaro.gonzalez@nao.ac.jp).

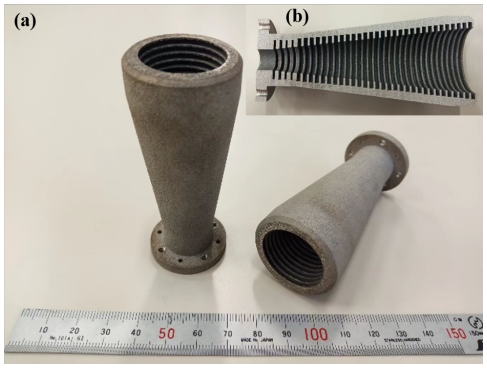

Fig. 1. (a) The as built wideband millimeter-wave corrugated horns fabricated by metal 3D printer (b) The cross section of one corrugated horn cut into two halves.

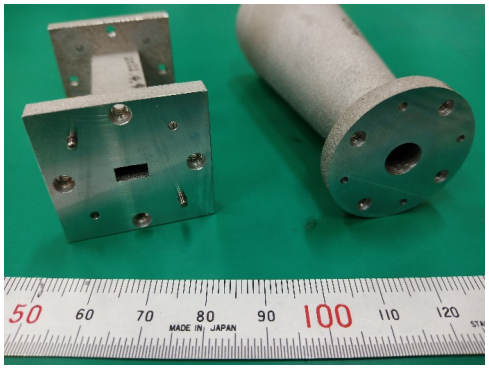

Fig. 2. The flange parts of both the WR-22 waveguide transition and the fabricated corrugated horn, which were post processed by milling machine.

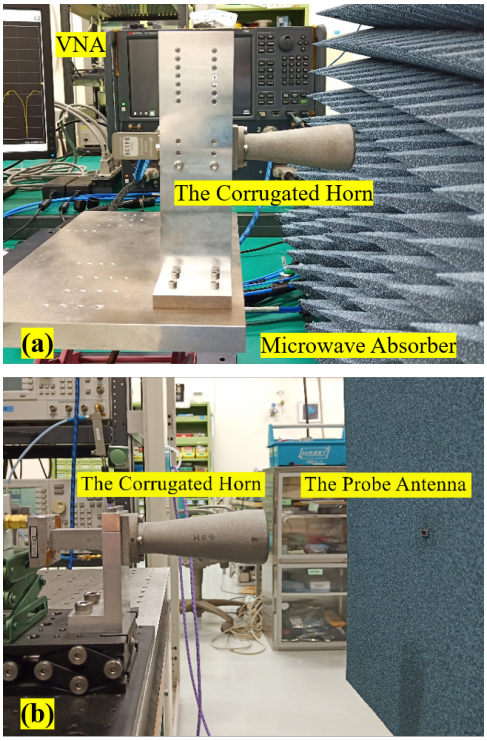

Fig. 3. The measurement setups for the designed corrugated horn (a) The S-parameter measurement setup (b) The near-field beam pattern measurement system at 30-50 GHz, the microwave absorber on the corrugated horn side has been removed in this figure for better viewing.

HE_{11} mode to the aperture of the corrugated horn, and this section is important for low XsP performance. For a compact corrugated horn design, we use an input circular waveguide with a radius of 3.65 mm and a 24 mm-diameter aperture. All the corrugations have a constant pitch of 2.16 mm, and the corrugated horn has 34 corrugations in total with a length of 79.3 mm.

The impedance of corrugated waveguide does not only depend on the ridge radius (r) and slot depth (s), but also the slot width (b). As discussed in [17], the corrugated waveguide with high ratio between slot depth (s) and slot width (b) has good broadband impedance matching, in other words, we need relatively thin and deep slots at the throat section. In [17], a linear taper of both the slot depth (s) and slot width (b) at throat section is used to realize broadband impedance matching. Thanks to development of modern EM simulation software, we use a commercial software WASP-NET [18] to fully optimize the depths and widths of the slots at the throat section instead. This software is based on a hybrid algorithm of Method of Moment (MoM) and Mode Matching (MM), and it supports fast optimization of corrugated horn parameters based on MM. In our design, we use the first 5 corrugations to realize the impedance matching and mode conversion. The optimized slot depths (s) are between 3.27 mm and 2.65 mm, which correspond to 0.44λ and 0.35λ at 40 GHz. The optimized slot widths (b) are between 0.67 mm and 1.34 mm with a largest depth/width ratio of 4.0, which is challenging with traditional fabrication techniques.

To improve the XsP performance, we use a profiled cross-section for the horn shape at the flare section. As discussed in [4], the slot depth (s) for minimum XsP of hybrid HE_{11} mode changes with the radius of corrugated waveguide. We further find that the values of slot depth (s) for minimum XsP can be fitted by a function with 3 parameters, the function is stated in (1),

$$s = a_1(\frac{2r}{\lambda})^{-a_2} + a_3 \quad (1)$$

where r is the radius of corrugated waveguide, λ is the wavelength. We firstly optimize the 3 parameters a_1, a_2 and a_3 in (1), and a maximum XsP lower than -30.7 dB has achieved in the whole frequency band. We continue trying to fine tune the slot profile for a better XsP performance, and we are able to reduce the maximum XsP to -32.0 dB. The final optimized slot depths (s) vary from 2.88 mm to 2.17 mm at the flare section, which correspond to 0.38λ to 0.29λ at 40 GHz.

III. Fabrication Based on Powder Bed Fusion

The designed corrugated horn has been fabricated by EOS M290 metal 3D printer with EOS $AlSi_{10}Mg$ material. This metal 3D printer is using laser-based PBF technology. The laser focus diameter is about 100 μm which results in fabrication tolerances around 100 μm. The average surface roughness (R_a) [19] of as built component is around 20 μm which is determined by the powder size (around 30 μm), laser

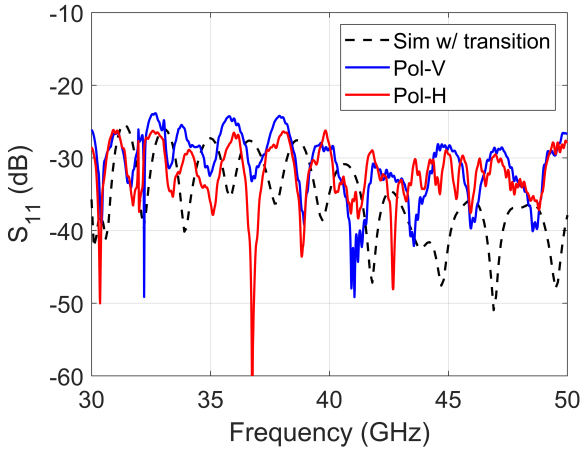

Fig. 4. The S_{11} measurement results for V and H polarizations.

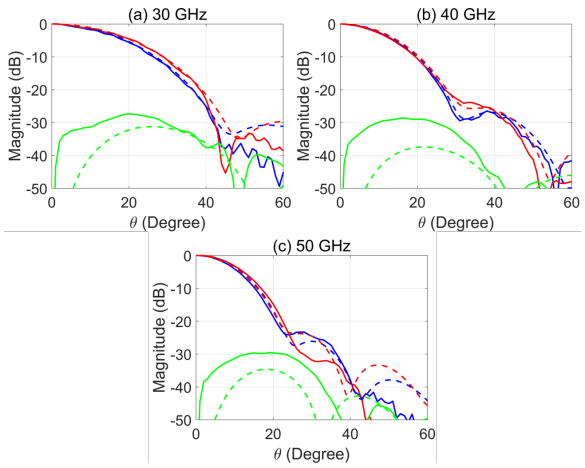

Fig. 5. The measured far-field beam patterns of the designed corrugated horn, H-plane CoP is in blue, E-plane CoP is in red, 45° XsP is in green, and solid lines are measurement results, dotted lines are simulation results (a) 30 GHz (b) 40 GHz (c) 50 GHz

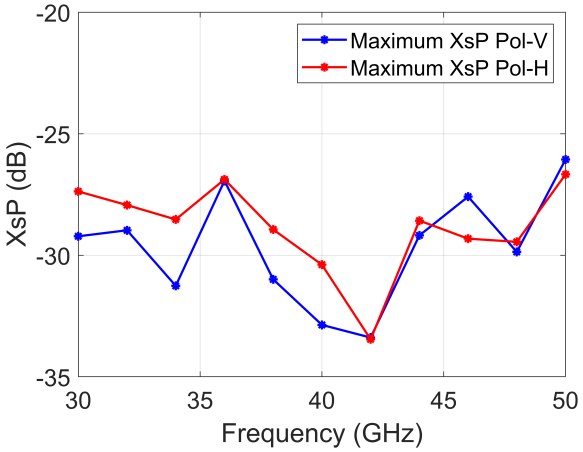

Fig. 6. The measured maximum Cross-Polarization (XsP) of the designed corrugated horn.

power and other printing parameters, and the current average surface roughness (R_a) is a optimal value after optimizations of fabrication process. Build orientation is at 45° with the build platform, and both internal and external support structures are used in the printing process to improve the fabrication accuracy of the corrugations.

The as built corrugated horns are shown in Fig. 1(a), and the cross section of one horn cut into two halves is shown in Fig. 1(b). It clearly shows that the first several thin corrugations are well fabricated by the metal 3D printer. The circular waveguide to WR-22 rectangular waveguide transition also has been fabricated to provide the necessary connection between the designed corrugated horn and measurement equipment.

The flange parts of both the fabricated corrugated horn and the WR-22 transition were post processed by milling machine to ensure the tight connection and accurate alignment between different waveguide components. They are important to avoid extra reflection between these components. Both 3D printing and post-processing procedure were conducted in Advanced Technology Center of the National Astronomical Observatory of Japan (NAOJ), and the delivery time of the designed corrugated horn has been further reduced thanks to the in-house fabrication.

IV. Corrugated Horn Characterization

The S-parameter of the fabricated corrugated horn has been measured by Keysight N5225B Vector Network Analyzer (VNA), and the measurement setup is shown in Fig. 3(a). The horn is connected to the VNA through a metal 3D printed WR-22 waveguide transition. All the components are assembled with an optical bench to maintain the stability during the measurement, and a microwave absorber is placed in front of the measurement setup to reduce the reflection from the environment. The measurement results of S_{11} for both Vertical (V) and Horizontal (H) polarizations are presented in Fig . 4, and WASP-NET simulation results with WR-22 transition are also included for comparison. The maximum S_{11} of both polarizations is -23.9 dB, which means a return loss better than 23.9 dB in the whole frequency band.

The beam patterns of the fabricated corrugated horn have been measured by a planar near-field measurement system [20], shown in Fig. 3(b). The corresponding far-field beam patterns was carefully calculated from the near-field measurement data based on the near-field-to-far-field transformation and probe calibration method reported in [21]. The Co-polarization (CoP) and Cross-polarization (XsP) far field beam patterns for V-polarization at three different frequencies are presented in Fig. 5. The measurement shows that the CoP beam patterns have good symmetric gaussian shape, but the XsP beam patterns have degradations due to the fabrication tolerances. The maximum XsP level is further presented in Fig. 6., this result shows that the maximum XsP in the whole frequency band is -26.1 dB. Although there are slight degradations compared with simulation, this value means an excellent polarization performance for most applications.

Both S-parameter and beam pattern measurements show that two orthogonal polarizations have slightly different performance which is due to the small asymmetry inside the corrugated horn. During the 3D printing process, the high-

power laser fuses the metal powder layer by layer in z-axis, and the build surface is perpendicular to z-axis of the machine coordinate system. It slightly introduces dimensional difference between V and H directions of the fabricated components which causes the un-symmetry inside the horn. This systematic error can be reduced by optimizing the 3D printing process, but it cannot be fully eliminated.

V. Conclusion

A wideband mm-wave corrugated horn at 30-50 GHz with a fractional bandwidth of 50% is designed and fabricated. The fabrication process is taking the advantage of commercial all-metal 3D printing technology to fabricate geometries which are challenging with traditional techniques, and also to reduce the cost and the delivery time. A return loss larger than 23.9 dB and maximum XsP lower than -26.1 dB in the whole frequency band have been verified by the measurements. This development of Q-band wideband corrugated horn can promote the application of wideband mm-wave corrugated horn in large array astronomical receivers, and it also has potential applications in Q-band satellite communication and remote sensing for meteorology.

Acknowledgments

The authors would like to thank Dr. H. Imada at NAOJ for the discussion on optimization for the performance of corrugated horns. We also would like to thank Mr. N. Arima at The University of Tokyo for editing support of this letter; Dr. M. Bao at Nanjing University for providing the slot depth data for minimum XsP.

References

[1] P. Clarricoats and P. Saha, "Propagation and radiation behaviour of corrugated feeds. part 2: Corrugated-conical-horn feed," in *Proceedings of the Institution of Electrical Engineers*, vol. 118, no. 9. IET, 1971, pp. 1177–1186.

[2] C. Dragone, "Reflection, transmission, and mode conversion in a corrugated feed," *The Bell System Technical Journal*, vol. 56, no. 6, pp. 835–867, 1977.

[3] ——, "Characteristics of a broadband microwave corrugated feed: A comparison between theory and experiment," *Bell System Technical Journal*, vol. 56, no. 6, pp. 869–888, 1977.

[4] P. J. B. Clarricoats and A. D. Olver, *Corrugated horns for microwave antennas*. Iet, 1984, no. 18.

[5] J. Carpenter, D. Iono, L. Testi, N. Whyborn, A. Wootten, and N. Evans, "The alma development roadmap," *arXiv preprint arXiv:1902.02856*, 2019.

[6] M. McKinnon, A. Beasley, E. Murphy, R. Selina, R. Farnsworth, and A. Walter, "ngvla: The next generation very large array," *Bulletin of the American Astronomical Society*, vol. 51, no. 7, p. 81, 2019.

[7] C. C. Chiong, "Ultimate receiver for 7mm frequency band : An overview on the eq receiver project," *The astronomical herald*, vol. 114, no. 4, pp. 281–288, 2021.

[8] F. Tercero, J. López-Pérez, J. Gallego, F. Beltrán, O. García, M. Patino-Esteban, I. López-Fernández, G. Gómez-Molina, M. Diez, P. García-Carreño *et al.*, "Yebes 40 m radio telescope and the broad band nanocosmos receivers at 7 mm and 3 mm for line surveys," *Astronomy & Astrophysics*, vol. 645, p. A37, 2021.

[9] A. Gonzalez, K. Kaneko, and S. Asayama, "Recent work on (sub-) mm-wave ultra wideband corrugated horns for radio astronomy," in *2017 11th European Conference on Antennas and Propagation (EUCAP)*. IEEE, 2017, pp. 3327–3331.

[10] J. Teniente, J. C. Iriarte, I. Ederra, and R. Gonzalo, "Advanced feeds for mm-wave antenna systems," in *Aperture Antennas for Millimeter and Sub-Millimeter Wave Applications*. Springer, 2018, pp. 75–110.

[11] W.-Y. Zhong, J. Dong, W. Gou, L.-F. Yu, J.-Q. Wang, B. Xia, W. Jiang, C. Liu, H. Zhang, J. Shi *et al.*, "A q-band two-beam cryogenic receiver for the tianma radio telescope," *Research in Astronomy and Astrophysics*, vol. 18, no. 4, p. 044, 2018.

[12] C.-C. Chiong, C. Chen, C.-T. Ho, S.-T. Jian, and Y.-J. Hwang, "A compact 30-50 ghz platelet corrugated feedhorn for cryogenic radio astronomical application," in *2020 50th European Microwave Conference (EuMC)*. IEEE, 2021, pp. 224–227.

[13] V. Bhavar, P. Kattire, V. Patil, S. Khot, K. Gujar, and R. Singh, "A review on powder bed fusion technology of metal additive manufacturing," *Additive manufacturing handbook*, pp. 251–253, 2017.

[14] A. Gonzalez, K. Kaneko, C.-D. Huang, and Y.-D. Huang, "Metal 3d-printed 35–50-ghz corrugated horn for cryogenic operation," *Journal of Infrared, Millimeter, and Terahertz Waves*, vol. 42, no. 9, pp. 960–973, 2021.

[15] T. Rossi, M. De Sanctis, M. Ruggieri, C. Riva, L. Luini, G. Codispoti, E. Russo, and G. Parca, "Satellite communication and propagation experiments through the alphasat q/v band aldo paraboni technology demonstration payload," *IEEE Aerospace and Electronic Systems Magazine*, vol. 31, no. 3, pp. 18–27, 2016.

[16] D. W. Draper, D. A. Newell, F. J. Wentz, S. Krimchansky, and G. M. Skofronick-Jackson, "The global precipitation measurement (gpm) microwave imager (gmi): Instrument overview and early on-orbit performance," *IEEE Journal of Selected Topics in Applied Earth Observations and Remote Sensing*, vol. 8, no. 7, pp. 3452–3462, 2015.

[17] X. Zhang, "Design of conical corrugated feed horns for wide-band high-frequency applications," *IEEE Transactions on Microwave Theory and Techniques*, vol. 41, no. 8, pp. 1263–1274, 1993.

[18] F. Arndt, "Wasp-net: Recent advances in fast em cad and optimization of waveguide components, feeds and aperture antennas," in *Proceedings of the 2012 IEEE International Symposium on Antennas and Propagation*. IEEE, 2012, pp. 1–2.

[19] H. Kalami and J. Urbanic, "Exploration of surface roughness measurement solutions for additive manufactured components built by multi-axis tool paths," *Additive Manufacturing*, vol. 38, p. 101822, 2021.

[20] A. Gonzalez, Y. Fujii, T. Kojima, and S. Asayama, "Reconfigurable near-field beam pattern measurement system from 0.03 to 1.6 thz," *IEEE Transactions on Terahertz Science and Technology*, vol. 6, no. 2, pp. 300–305, 2016.

[21] H. Kang, A. Gonzalez, R. Sakai, and K. Kaneko, "Accurate Reconstruction of Far-Field Polarization Beam Patterns from Planar Near-Field Measurements," 3 2022. [Online]. Available: https://www.techrxiv.org/articles/preprint/Accurate_Reconstruction_of_Far-Field_Polarization_Beam_Patterns_from_Planar_Near-Field_Measurements/19365545